Eighth International Conference on
THIN-WALLED STRUCTURES – ICTWS 2018
Lisbon, Portugal, July 24-27, 2018

CREEP ANALYSIS OF STEEL-CONCRETE COMPOSITE BEAMS USING GENERALIZED BEAM THEORY

David Henriques*, Rodrigo Gonçalves and Dinar Camotim*****

* TECNORÉM S.A., Estrada Nacional 113, Moinho da Areia, 2490-444 Ourém, Portugal
e-mail: dos.santos.henriques.david@gmail.com

** CERIS, ICIST and DEC/FCT, Universidade Nova de Lisboa, 2829-516 Caparica, Portugal
e-mail: rodrigo.goncalves@fct.unl.pt

*** CERIS, ICIST, DECivil, Instituto Superior Técnico, Universidade de Lisboa, 1049-001 Lisbon, Portugal
e-mail: dcamotim@civil.ist.utl.pt

Keywords: Steel-concrete beams; Shear lag; Creep; Generalized Beam Theory.

Abstract. *This paper presents the latest developments concerning the numerical modelling of steel-concrete composite beams using finite elements based on Generalized Beam Theory (GBT). In particular, this paper is dedicated to showing that GBT makes it possible to obtain, with significant accuracy and computational efficiency, the combined effects of creep and shear lag. In order to capture these effects, shear lag deformation modes are added to the beam kinematic description and the influence of creep is taken into account through a linear viscoelastic law which is written as a Dirichlet series expansion. An illustrative numerical example is presented, to show the capabilities and potential of the proposed GBT-based finite element formulation.*

1 INTRODUCTION

Generalized Beam Theory (GBT) is a thin-walled prismatic bar theory that handles, with great accuracy and computational efficiency, cross-section in-plane and out-of-plane (warping) deformation, through the inclusion of hierarchical and structurally meaningful cross-section DOFs, the so-called "cross-section deformation modes". Since its original form [1,2], GBT has been considerably developed and is presently established as a very efficient and valuable numerical tool to analyze the structural behavior of thin-walled bars (e.g., [3-5]).

GBT was first applied in the field of steel-concrete composite beams/bridges in [6], where it was shown that it can handle, with great efficiency, complex effects such as cross-section distortion, the presence of transverse diaphragms, shear lag and shear connection flexibility. In this first paper, several examples were presented concerning linear elastostatic and undamped free vibration analyses, and semi-analytical buckling solutions were provided for simply supported members under uniform negative moment.

Quite recently, in [7], the authors proposed a very accurate and efficient physically non-linear GBT-based beam finite element, which can capture the materially non-linear behavior of wide-flange steel and steel-concrete composite beams up to collapse. This finite element incorporates the effects of concrete cracking/crushing, shear lag in wide flanges and steel plasticity. In particular, the element can offer significant advantages, with respect to standard shell/solid finite element and finite strip models, since (i) semi-analytical solutions can be obtained in particular cases, (ii) a much smaller number of DOFs is generally required to achieve accurate results, even in full numerical analyses, (iii) the computation times are greatly reduced, particularly in physically non-linear problems, and (iv) the GBT modal decomposition of the solution into hierarchic and structurally meaningful cross-section

deformation modes provides invaluable insight into the mechanics of the problems under consideration.

Finally, in [8], the authors proposed another GBT-based finite element for calculating buckling (bifurcation) loads of steel-concrete composite beams. This element accounts for shear lag, concrete cracking and distortional/local buckling effects. In particular, the intrinsic versatility of the GBT approach, allowing the incorporation of a relatively wide range of assumptions, led to a finite element with a reasonably small number of DOFs and, most importantly, to an element which can comply with the principles of the "inverted U-frame" model prescribed in Eurocode 4 [9].

In the present paper, the newest developments in this field are presented. A new finite element is proposed, which can combine the effects of creep and shear lag in a very efficient way. The creep effects are modelled using a viscoelastic law and its expansion into a Dirichlet series, as proposed in [10], and the shear lag effects are considered through the introduction of linear, quadratic, cubic and quartic warping functions in the concrete slab. In the near future, this new element will be enhanced to account for the effects of shear connection flexibility (as already presented in [6]), cracking and shrinkage.

It is worth mentioning that there are already several finite elements capable of capturing time-dependent effects in steel-concrete composite beams, as presented in the state-of-the-art paper [11], which describes the major developments up to 2013. Here, only the papers that allow for shear lag and creep (thus being more related to the present work), are mentioned. In this respect, to the authors best knowledge, two papers are of particular interest: (i) [12], where a beam finite element is presented that can account for shear connection flexibility, time-dependent effects (using an integral-type approach with the trapezoidal rule) and shear-lag (using a single warping function), and (ii) [13], in which case analytical solutions are provided for a model quite similar to that in [12].

The notation introduced in [14,15] is followed, with a set of auxiliary matrices denoted by the symbol $\boldsymbol{\Xi}$. Bold letters are employed to designate matrices and vectors, the comma indicates a partial derivative (e.g., $f_{,x} = \partial f/\partial x$), although the dot is reserved for a time derivative ($\dot{f} = df/dt$). Finally, the superscripts $(\cdot)^M$ and $(\cdot)^B$ designate plate-like membrane and bending components, respectively.

2 FORMULATION AND FINITE ELEMENT IMPLEMENTATION

2.1 Kinematic description

The beam cross-section considered is as shown in Fig. 1(a), with a reinforced concrete slab and an I-section steel beam. Fig. 1(b) displays the wall mid-lines and cross-section in-plane local axes y and z (x defines the beam longitudinal direction), which constitute the basis of the GBT kinematic description. Each reinforcement layer is assumed smeared and no slip rebars and concrete is allowed. The cross-section is subdivided into: (i) two flanges and one web, for the steel I-section, and (ii) two reinforced concrete flanges of widths b_{c1} and b_{c2}. The parameters associated with the concrete slab, steel I-section beam and rebars are identified by the subscripts c, a and s, respectively.

The standard GBT variable separation technique is employed for expressing the membrane displacements (u, v, w), along (x, y, z), respectively, namely

$$u = \overline{\boldsymbol{u}}^T(y)\,\boldsymbol{\phi}_{,x}(x), \qquad v = \overline{\boldsymbol{v}}^T(y)\,\boldsymbol{\phi}(x), \qquad w = \overline{\boldsymbol{w}}^T(y)\,\boldsymbol{\phi}(x), \tag{1}$$

where $\overline{\boldsymbol{u}}, \overline{\boldsymbol{v}}, \overline{\boldsymbol{w}}$ are column vectors that collect the mid-line displacement components of the cross-section deformation mode functions and $\boldsymbol{\phi}$ is a column vector containing their respective amplitude functions, which are the problem unknowns. Kirchhoff's thin-plate assumption is adopted, meaning that the displacements of each wall may be completely written in terms of the membrane displacements and plate-like shear locking is *a priori* eliminated. For small displacements, the displacement vector $\boldsymbol{U}$ reads

$$\boldsymbol{U} = \begin{bmatrix} U_x \\ U_y \\ U_z \end{bmatrix} = \boldsymbol{\Xi}_U \begin{bmatrix} \boldsymbol{\phi} \\ \boldsymbol{\phi}_{,x} \end{bmatrix}, \quad \boldsymbol{\Xi}_U = \begin{bmatrix} \mathbf{0} & \overline{\boldsymbol{u}}^T - z\overline{\boldsymbol{w}}^T \\ \overline{\boldsymbol{v}}^T - z\overline{\boldsymbol{w}}_{,y}^T & \mathbf{0} \\ \overline{\boldsymbol{w}}^T & \mathbf{0} \end{bmatrix}. \tag{2}$$

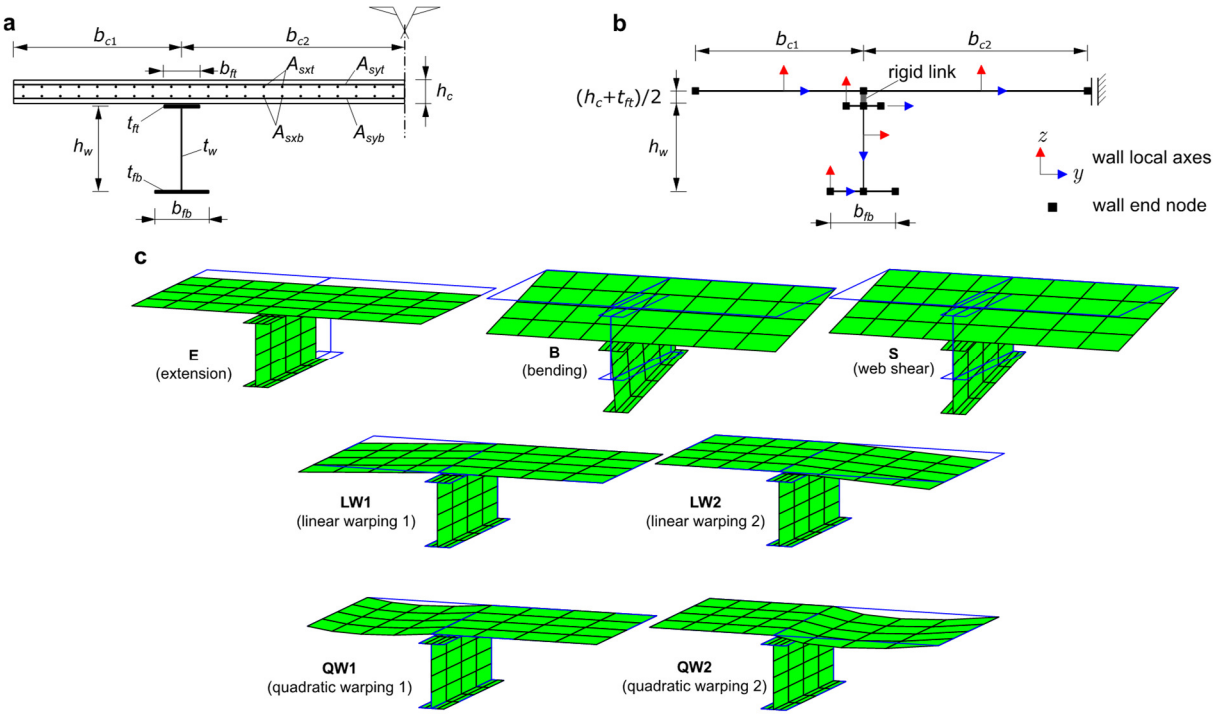

Figure 1: Steel-concrete composite beam (a) cross-section geometry, (b) wall mid-lines and boundary conditions, and (c) cross-section deformation modes.

The strains are straightforwardly obtained from the displacements and may also be subdivided into membrane and bending components, reading

$$\boldsymbol{\varepsilon} = \begin{bmatrix} \varepsilon_{xx} \\ \varepsilon_{yy} \\ \gamma_{xy} \end{bmatrix} = \boldsymbol{\varepsilon}^M + \boldsymbol{\varepsilon}^B = \boldsymbol{\Xi}_\varepsilon \begin{bmatrix} \boldsymbol{\phi} \\ \boldsymbol{\phi}_{,x} \\ \boldsymbol{\phi}_{,x} \end{bmatrix}, \; \boldsymbol{\Xi}_\varepsilon = \boldsymbol{\Xi}_\varepsilon^M + \boldsymbol{\Xi}_\varepsilon^B, \; \boldsymbol{\Xi}_\varepsilon^{(\cdot)} = \begin{bmatrix} \mathbf{0} & \mathbf{0} & \left(\boldsymbol{\xi}_{13}^{(\cdot)}\right)^T \\ \left(\boldsymbol{\xi}_{21}^{(\cdot)}\right)^T & \mathbf{0} & \mathbf{0} \\ \mathbf{0} & \left(\boldsymbol{\xi}_{32}^{(\cdot)}\right)^T & \mathbf{0} \end{bmatrix}, \tag{3}$$

where $\boldsymbol{\xi}_{ij}^{(\cdot)}$ are the following column vectors

$$\boldsymbol{\xi}_{13}^M = \overline{\boldsymbol{u}}, \qquad \boldsymbol{\xi}_{13}^B = -z\overline{\boldsymbol{w}}, \tag{4}$$

$$\boldsymbol{\xi}_{21}^M = \overline{\boldsymbol{v}}_{,y} \qquad \boldsymbol{\xi}_{21}^B = -z\overline{\boldsymbol{w}}_{,yy}, \tag{5}$$

$$\boldsymbol{\xi}_{32}^M = \overline{\boldsymbol{v}} + \overline{\boldsymbol{u}}_{,y}, \qquad \boldsymbol{\xi}_{32}^B = -2z\overline{\boldsymbol{w}}_{,y}. \tag{6}$$

The stresses $\boldsymbol{\sigma}^{\mathrm{T}} = [\sigma_{xx}\ \ \sigma_{yy}\ \ \sigma_{xy}]$ are obtained from the previous strains, using the appropriate constitutive relations, as discussed in Section 2.2.

In the present work, since one is aiming at modelling shear lag and creep effects, the assumptions adopted in [7] are followed, namely: (i) the cross-section is in-plane undeformable and cannot twist, meaning that $\varepsilon_{yy} = \gamma_{xy}^{B} = 0$, and (ii) Vlasov's assumption ($\gamma_{xy}^{M} = 0$) is enforced in the narrow steel flanges, i.e., membrane shear deformation is only allowed in the concrete slab, to capture shear lag, and in the steel web. Due to these constraints, only a few cross-section deformation modes need to be included in the analyses. These modes are shown in Fig. 1(c) (only the wall mid-lines are represented): (E) axial extension, (B) Euler-Bernoulli bending assuming uncracked concrete, (S) steel web constant shearing and (LW/QW) linear/quadratic shear lag warping modes in each concrete flange. Furthermore, cubic and quartic shear lag warping modes are also considered in the present paper, to investigate whether they enhance slightly the results obtained. Note that, although no axial force will be applied at the cross-section in the example presented in Section 3 of this paper, the E mode must be included in the analyses to capture the shift of the neutral line due to shear lag and creep effects (and also cracking, which is not considered in the present paper). For symmetric concrete flanges, the shear lag warping modes may be paired due to symmetry, and the number of cross-section DOFs can be reduced.

2.2 Constitutive relations

Due to the assumptions introduced, only the stress components $\sigma_{xx},\ \sigma_{xy}^{M}$ are taken into account and $\sigma_{yy} = 0$ is assumed. For steel, these stresses are related to the strains through

$$\sigma_{xx} = E\varepsilon_{xx},\ \ \sigma_{xy}^{M} = G\gamma_{xy}^{M}, \tag{7}$$

where E is Young's modulus and G is the shear modulus.

For concrete, the standard integral equation for linear viscoelasticity is adopted, reading, for the strain at time t,

$$\varepsilon(t) = J(t)\sigma(0) + \int_0^t J(t-\tau)\,\dot{\sigma}(\tau)\mathrm{d}\tau, \tag{8}$$

where J is the creep function. A Dirichlet series expansion of the creep function is followed, leading to

$$J(t-\tau,\tau) = \frac{1}{E_0} + \sum_{\alpha=1}^{n} \frac{1}{E_\alpha}\left[1 - e^{-\frac{t-\tau}{\lambda_\alpha}}\right], \tag{9}$$

which can be viewed as a chain of Kelvin spring-dashpot elements, each with spring stiffness E_α and retardation time λ_α. Assuming a constant stress variation within a time step and isotropy, the time integration of the constitutive relation leads to an incremental relation which reads, for the relevant stress components of the case under consideration,

$$\begin{bmatrix}\Delta\sigma_{xx}\\ \Delta\sigma_{xy}^{M}\end{bmatrix} = \left(\frac{1}{E_0} + \sum_{\alpha=1}^{n}\frac{1}{E_\alpha}\left[1 - \frac{\lambda_\alpha}{\Delta t}\left(1 - e^{-\frac{\Delta t}{\lambda_\alpha}}\right)\right]\right)^{-1}\begin{bmatrix}1 & 0\\ 0 & \frac{1}{2(1+\nu)}\end{bmatrix}$$
$$\left(\begin{bmatrix}\Delta\varepsilon_{xx}\\ \Delta\gamma_{xy}^{M}\end{bmatrix} - \sum_{\alpha=1}^{n}\boldsymbol{\varepsilon}_\alpha^{*}(t-\Delta t)\left(1 - e^{-\frac{\Delta t}{\lambda_\alpha}}\right)\right), \tag{10}$$

where $\boldsymbol{\varepsilon}_\alpha^{*}$ are state variables which are updated at the end of each step and read

$$\boldsymbol{\varepsilon}_{\alpha}^{*}(t) = e^{-\frac{\Delta t}{\lambda_{\alpha}}}\,\boldsymbol{\varepsilon}_{\alpha}^{*}(t-\Delta t) + \frac{\lambda_{\alpha}}{\Delta t E_{\alpha}}\left(1 - e^{-\frac{\Delta t}{\lambda_{\alpha}}}\right)\Delta\boldsymbol{\sigma}. \tag{11}$$

2.3 Finite element implementation

The finite element employed is similar to that in [7], where the deformation mode amplitude functions are approximated using Hermite cubic and Lagrange quadratic functions, the latter for the deformation modes that exclusively involve warping (the extension mode and the shear lag warping modes). With the deformation modes shown in Fig. 1c, the finite element has a total of 2×4 + 5×3 = 23 DOFs. For each additional shear lag warping mode (cubic or quartic), 3 DOFs are added.

The stiffness matrix is straightforwardly obtained from the virtual work principle, using the strains given by Eqs. (3) and the elastic (for steel) and viscoelastic (for concrete) constitutive relations previously discussed. The external load vector is obtained from the external virtual work, using the displacements (2) and also the term of Eq. (10) that does not depend on the incremental strains. The longitudinal integration (along x) is carried out with 3 Gauss points and the cross-section integration involves three points along y (mid-line direction) and 2 points along z (through-thickness direction).

The incremental procedure is carried out step by step, calculating the resulting incremental displacements and updating the state variables. The finite element procedure was implemented in MATLAB [16]. Concerning the computation times, with an Intel Core i7 4700HQ CPU @ 2.40 GHz, the runtime for a single finite element with four shear lag warping modes and 14 time steps is about 1.3 seconds. Increasing the discretization to eight finite elements increases the runtime to about 5.6 seconds, which is still quite fast.

3 ILLUSTRATIVE EXAMPLE

The illustrative example considered corresponds to a simply supported 8 m span steel-concrete composite beam, subjected to a 1 kN/m uniformly distributed load applied above the steel web. The cross-section is as shown in Fig. 1a, without rebars and with the following geometric parameters (mm): h_c = 200, b_{c1} = 1500, b_{c2} = 2000, t_f = 30, t_w =15, b_f = 300 and h_w = 770. The elastic material properties are: E_s = 210 GPa, ν_s = 0.3, E_c = 37 GPa and ν_c = 0.1. The Eurocode 2 [18] creep function is adopted, with: t_0 = 14 days, f_{cm} = 28 MPa and RH = 80 %. The coefficients of the series expansion of the creep function are obtained using the least squares method and are provided in Table 1. A comparison between the creep function and the series expansion adopted is depicted in the graph of Fig. 2 (the data points are indicated by the circles), attesting a virtual exact match.

The GBT analyses are carried out considering the problem symmetry (i.e., only half of the span is modelled). The influence of the number of finite elements, deformation modes and time steps is assessed next.

For comparison purposes, a refined shell finite element model was analyzed in ADINA [17], using 4-node MITC elements. The model is shown in Fig. 2 and also takes advantage of the problem symmetry. Since no longitudinal slip is allowed in the steel-concrete interface, the connection between the mid-surfaces of the concrete slab and steel top flange is materialized through rigid links. To use the ADINA viscoelastic material law, the relaxation function or its series expansion must be provided. The calculation of the relaxation data from the creep function was obtained by simulating a relaxation test and integrating the resulting equation using a simple Euler forward scheme and very small time steps. Then, 15

coefficients for the Dirichlet series expansion of the relaxation function were adopted, being calculated with the least squares method.

Table 1: Coefficients of the series expansion of the creep function.

α	E_α (kPa)	λ_α (days)
0	3.638E7	-
1	7.131E8	1E−3
2	1.136E9	1E−2
3	2.514E8	1E−1
4	2.058E8	1
5	6.964E7	1E1
6	4.621E7	1E2
7	1.132E8	4E2
8	1.381E8	1E3
9	5.816E8	3E3
10	1.228E9	1E4
11	1.370E9	1E5

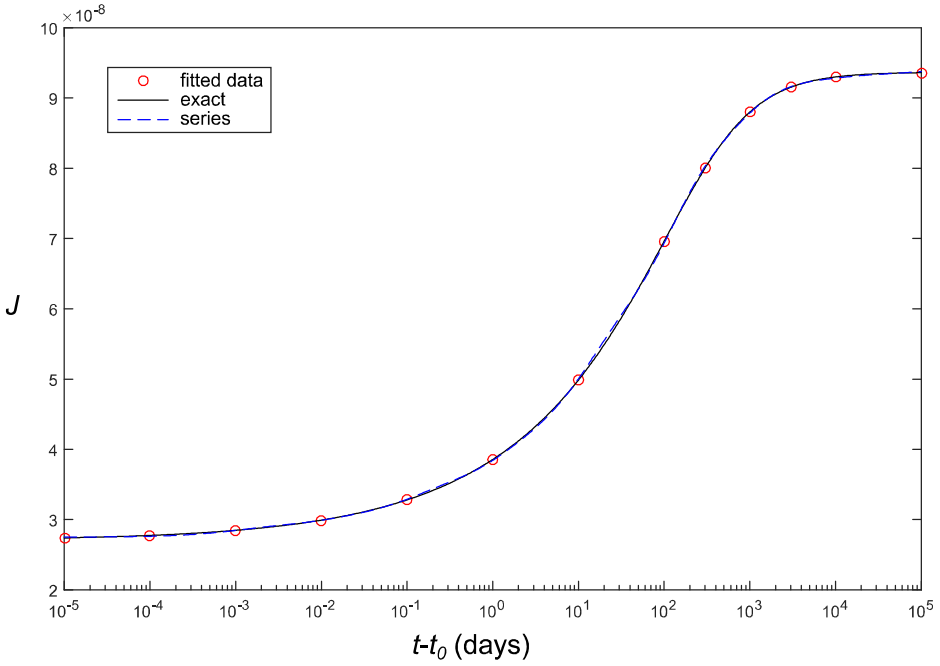

Figure 2: Creep function adopted and corresponding series approximation.

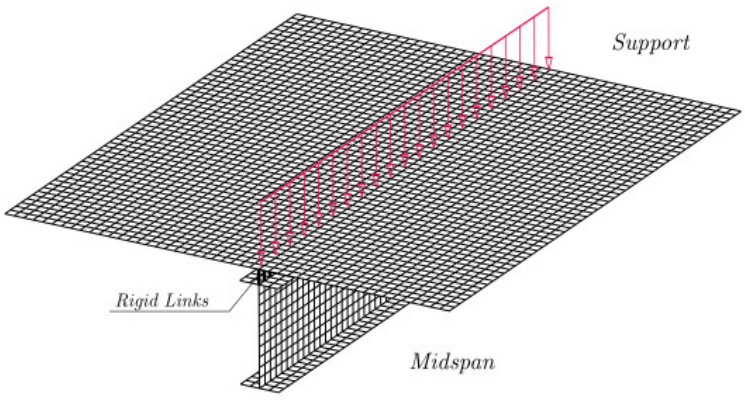

Figure 3: Shell finite element model.

First, the number of GBT-based finite elements is varied. For $t - t_0 = 0$ the mid-span vertical displacement with a single element equals 0.0352 mm, which is remarkably within 0.6 % of the result obtained with the shell model (0.0354 mm). The GBT results change very slightly when the number of GBT elements is increased.

For $t - t_0 = 1E6$ days, using 14 time steps of constant interval in logarithmic scale and a single GBT element, the differences are higher, with 0.04432 mm in the GBT model and 0.0454 mm in the shell model, amounting to a 2.4 % difference (still remarkably small). This difference does not change if more GBT finite elements are considered.

Fig. 4 displays the evolution of the mid-span displacement with time, obtained with (i) five GBT-based finite elements and 14 time steps, and (ii) the shell finite element model. A very good match is observed, with the maximum difference of 2.6 % at $t - t_0 = 1E4$ days. If a single time step is considered in the GBT analysis, the maximum displacement is 0.0441 mm, a value which falls within only 0.3 % of that obtained with 14 time steps.

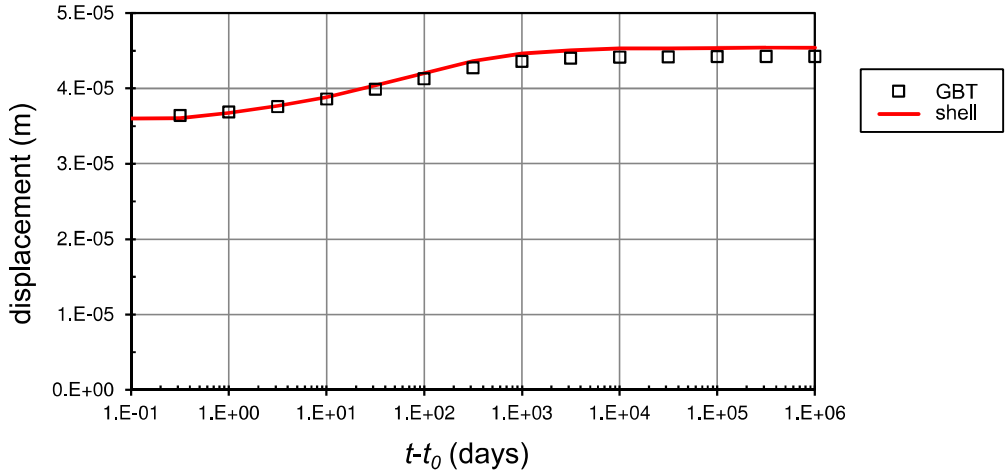

Figure 4: Evolution of the mid-span vertical displacement with time.

Fig. 5 shows the mid-span longitudinal strains at the concrete slab mid-line (i.e., $z = 0$), for $t = t_0$ and $t = \infty$, obtained with the shell model and eight GBT finite elements. For $t = \infty$, two GBT analyses are carried out, using either four (linear and quadratic) or eight (linear, quadratic, cubic and quartic) shear lag deformation modes.

For $t = t_0$ a virtually perfect match between the GBT and shell models is obtained, with differences below 1 %, making it possible to conclude that it suffices to consider only the first four shear lag deformation modes (linear and quadratic). However, for $t = \infty$, using four shear lag modes leads to a difference of about 5.4 % (near $y = 0$); if eight shear lag modes are used instead, this maximum difference drops to 2.6 %, but the maximum strains, above the steel web ($y = 1.5$ m), are slightly underestimated.

Finally, Fig. 6 displays the amplitude functions of each GBT cross-section deformation mode between the left support and mid-span ($x = 4$ m), considering eight finite elements and only the LW and QW shear lag warping modes, for both $t = t_0$ and $t = \infty$. These results prompt the following remarks:

(i) The most relevant mode is bending (B), which is maximum at mid-span and null at the supports, and its value increases with time. The second most relevant mode is the S shear mode, whose higher participation occurs at mid-span – note that web shear deformation is proportional to the derivative of this amplitude function, being maximum at the supports and null at mid-span. However, it is observed that the amplitude of this shear mode virtually does not vary over time.

(iii) The warping modes (E, LW, QW) have significantly lower participations, with the LW modes being the most relevant, followed by the E mode. The shear lag warping modes are related to the occurrence of shear deformation, like the S mode, and therefore their amplitude functions $\phi_{k,x}$ are maximum at the supports and null at mid-span. Naturally, their participations also increase over time.

(iv) It is also worth noting that the participations of the shear lag modes for the wider concrete flange (LW2 and QW2) are higher than their narrower flange counterparts (LW1 and QW1), which is due to the cross-section asymmetry and is in accordance with the mid-span longitudinal strain distribution shown in Fig. 5.

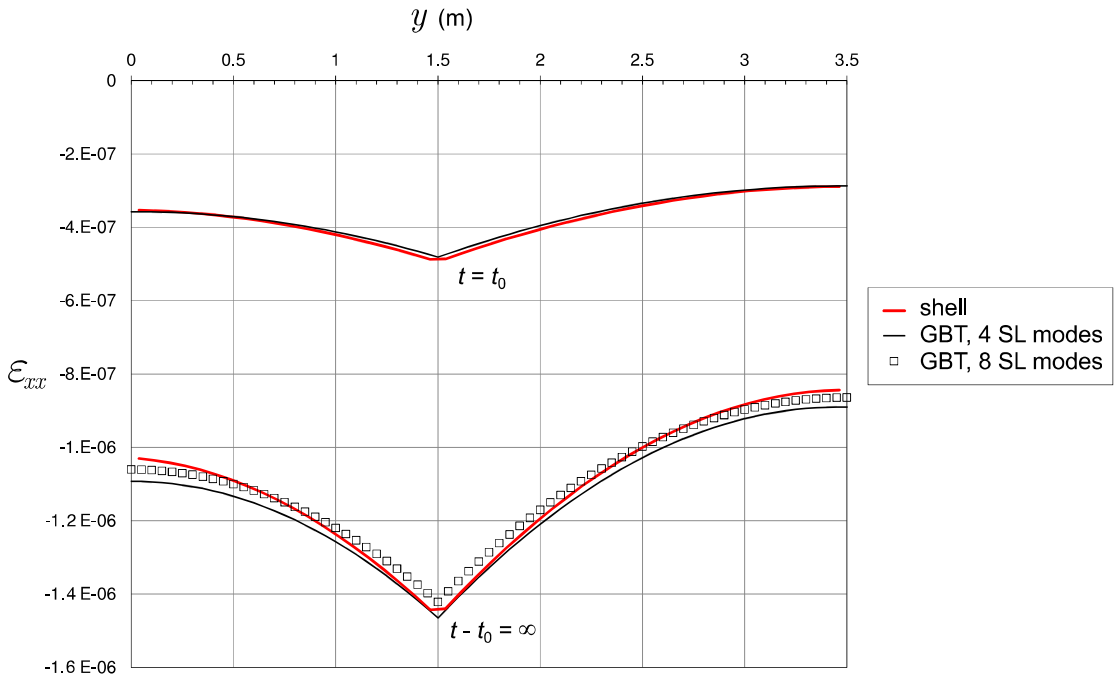

Figure 5: Mid-span longitudinal strains in the concrete slab mid-line.

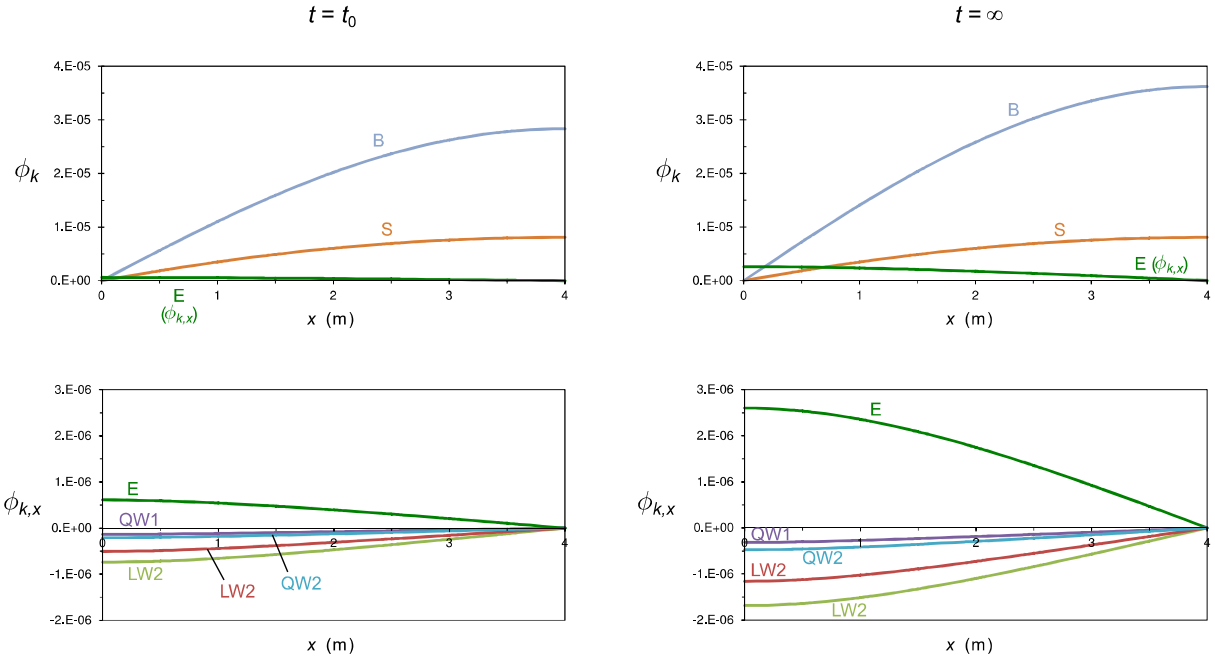

Figure 6: Amplitude functions for $0 \leq x \leq 4$ m, at $t = t_0$ and $t = \infty$.

4 CONCLUSION

This paper presented a very efficient GBT-based finite element which combines the effects of creep and shear lag in steel-concrete composite beams. Creep is modelled using a linear viscoelastic constitutive model and a Dirichlet series expansion of the creep function, whereas the shear lag effect is considered through the introduction of linear, quadratic, cubic and quartic warping functions in the concrete slab.

An illustrative example was presented, concerning a simply supported steel-concrete composite beam with unequal concrete flanges and subjected to a uniformly distributed vertical load. The comparison of the results obtained with the proposed beam finite element and those obtained with a refined shell finite element model show that the proposed element leads to very accurate results despite the reduced number of DOFs involved. In particular, it was shown that a single finite element already leads to excellent results and that the cubic and quartic shear lag modes only improve the results marginally.

Future developments, which will be reported in the near future, include the enhancement of the proposed finite element to account for the effects of shear connection flexibility, cracking and shrinkage.

REFERENCES

[1] Schardt R., "Eine erweiterung der technischen biegetheorie zur berechnung prismatischer faltwerke", *Stahlbau*, **35**, 161-171, 1966 (German).

[2] Schardt R., *Verallgemeinerte Technische Biegetheorie*, Springer Verlag, Berlin, 1989 (German).

[3] Camotim D., Basaglia C., Bebiano R., Gonçalves R., Silvestre N., "Latest developments in the GBT analysis of thin-walled steel structures", *Proceedings of Int. Colloquium on Stability and Ductility of Steel Structures*, E. Batista et al. (eds.), Rio de Janeiro, Brazil, 33-58, 2010.

[4] Camotim D., Basaglia C., Silva N., Silvestre N., "Numerical analysis of thin-walled structures using Generalised Beam Theory (GBT): Recent and future developments", *Computational Technology Reviews*, B. Topping et al. (eds.), Saxe-Coburg, Stirlingshire, 315-354, 2010.

[5] Camotim D., Basaglia C., "Buckling analysis of thin-walled steel structures using Generalized Beam Theory (GBT): state-of-the-art report", *Steel Construction*, **6**(2), 117-131, 2013.

[6] Gonçalves R., Camotim D. "Steel-concrete composite bridge analysis using Generalised Beam Theory", *Steel and Composite Structures*, **10**(3), 223-43, 2010.

[7] Henriques D., Gonçalves R., Camotim D. "A physically non-linear GBT-based finite element for steel and steel-concrete beams including shear lag effects", *Thin-Walled Structures*, **90**, 202-215, 2015.

[8] Henriques D., Gonçalves R., Camotim D. "GBT-based finite element to assess the buckling behavior of steel-concrete composite beams", *Thin-Walled Structures*, **107**, 207-220, 2016.

[9] EN1994-1-1:2004, *Eurocode 4: Design of Composite Steel and Concrete Structures. Part 1-1: General Rules and Rules for Buildings*, CEN, Brussels, Belgium, 2004.

[10] Bažant Z., Wu S. "Dirichlet series creep function for aging of concrete", *Journal of the Engineering Mechanics Division*, **9**(2), 367-387, 1973.

[11] Ranzi G., Leoni G., Zandonini R., "State of the art on the time-dependent behaviour of composite steel-concrete structures", *Journal of Constructional Steel Research*, **80**, 252-263, 2013.

[12] Gara F., Leoni G., Dezi L., "A beam finite element including shear lag effect for time-dependent analysis of steel-concrete composite decks", *Engineering Structures*, **31**, 1888-902, 2009.

[13] Zhu L., Su R., "Analytical solutions for composite beams with slip, shear-lag and time-dependent effects", *Engineering Structures*, **152**, 559-578, 2017.

[14] Gonçalves R., Ritto-Corrêa M., Camotim D., "A new approach to the calculation of cross-section deformation modes in the framework of Generalized Beam Theory", *Computational Mechanics*, **46**(5), 759-781, 2010.

[15] Gonçalves R., Camotim D., "Geometrically non-linear Generalised Beam Theory for elastoplastic thin-walled metal members", *Thin-Walled Structures*, **51**, 121-129, 2012.

[16] MATLAB, *version 7.10.0 (R2010a)*, The MathWorks Inc., Massachusetts, 2010.

[17] Bathe K. J., *ADINA System*, ADINA R&D Inc., 2017.

[18] EN1992-1-1:2004, *Eurocode 2: Design of Concrete Structures. Part 1-1: General Rules and Rules for Buildings*, CEN, Brussels, Belgium, 2004.